ULTRASHORT OPTICAL PULSES IN THE LINAC COHERENT LIGHT SOURCE

V. Bharadwaj, A. Chao, M. Cornacchia, P. Emma, T. Kotseroglou, P. Krejcik, I. Lindau, H-D. Nuhn, G. Stupakov, R. Tatchyn; Stanford Linear Accelerator Center.

R. Bionta, A. Toor; Lawrence Livermore National Laboratory.

C. Pellegrini; University of California at Los Angeles.

July 25, 2000

Abstract: *The Linac Coherent Light Source (LCLS) project at the Stanford Linear Accelerator Center (SLAC) will produce intense, coherent 0.15 nm x-rays, with an expected peak brightness many orders of magnitude greater than existing x-ray sources and energy density as high as 4 x 10^{25} watts/cm^2. These x-rays are produced by a single pass of a 15 GeV electron beam through a long undulator. The 15 GeV electron beam is generated using the last one third of the existing SLAC linac. This paper describes how to extend the present design of the LCLS to generate even shorter x-ray pulses than the nominal 255 femtoseconds FWHM. The goal of this study is to obtain pulse lengths as short as 50 femtoseconds. The scientific need for the shorter bunches is outlined, and electron and x-ray pulse compression options are reviewed. The analysis concludes that there are paths, albeit difficult, to obtaining shorter bunches and that the present LCLS design has the flexibility and range to test these paths.*

Table of Contents:

1. Scientific Need

The development and use of short light pulses have been intimately coupled to progress in laser technology. Shortly after the invention of the laser in the sixties it was used to create microsecond and nanosecond pulses. A variety of new research areas and applications opened up. In the seventies laser physics got into the picosecond (ps) time-regime and the femtosecond (fs) barrier was broken in the eighties, both with major impact on research. Presently attosecond lasers are pursued vigorously.

The need to produce pulses on the femtosecond timescale cuts across many disciplines in fundamental and applied sciences, the main reason being that many electronic processes occur in this timescale. Electron transfer reaction dynamics in atomic and molecular systems, providing information about the most basic reaction mechanisms (e.g. forming and breaking chemical bonds) in chemistry, biology and soft/condensed matter physics are on the femtosecond scale.

Synchrotron radiation is used by a very broad scientific community and the time structure provided (from the infrared to hard x-rays) is an important aspect for many applications. However, it is very hard to get pulses shorter than 30-50 ps without seriously sacrificing other performance parameters of the synchrotron radiation. The baseline design of LCLS with a nominal 255 fs (this value is used, as opposed to the LCLS Design Study Report's [1] design pulse length of 233 fs throughout this report due to changes in the design reflected in Ref. [2]) pulse structure is thus two orders of magnitude shorter than the-start-of-the-art of the most modern synchrotron radiation sources. This is, in itself, a most significant advance that will open up novel scientific opportunities. There are certainly a number of alternate schemes to produce femtosecond x-ray pulses. However, the femtosecond time-structure, in combination with the other characteristics of the LCLS pulse: high peak brilliance, full coherence and energy tunability, make the LCLS a unique photon source.

Historically it is seen that each advance with lasers towards shorter pulses has made possible new scientific research. This will certainly also be the case for the LCLS. From the LCLS workshops [3] it is clear that an improvement from 255 to 50 fs in optical pulse length will have a major impact on at least two general areas of research. Molecular vibrations have typical lifetimes of a few hundred femtoseconds. With probing pulses of 50 fs these excitations will appear basically as frozen. This will facilitate and make it possible to study fundamental, dynamical excitation mechanisms in conjunction with, for instance, structure determinations. Furthermore, a 50 fs pulse (as compared to 255 fs) is more advantageous for structure determinations of biomolecular fragments and single

biomolecules. Detailed simulations, with the relevant LCLS parameters, also provide clear evidence that the radiation damage is a much less severe problem for the shorter pulses.

Undoubtedly, the scientific communities will keep asking for shorter and shorter pulses. The realization of 50 femtosecond LCLS x-ray pulses will be tremendously important for some classes of experiments and significantly enhance the future capabilities of LCLS.

2. Overview of Compression Techniques

The primary purpose of the electron bunch compression system in the LCLS is to increase the bunch current so that SASE conditions are achieved. This increase in peak current is accomplished by reducing the electron bunch length from the 10 ps at the gun, down to 255 fs (FWHM) at the exit of the second bunch compressor. The resulting shorter x-ray pulse has the additional benefits of being brighter and more useful for scientific experiments. Section 1 discussed the scientific merits of further decreasing the FEL pulse length down to 50 fs and below. In response to these scientific requirements, the authors of this paper have explored the possibility of reducing the electron and/or the x-ray pulse length below the 255 fs value chosen in the LCLS Design Study [1,2]. It is understood that achieving the reference value will, in itself, present a considerable challenge, and that the planned initial experiments will have to be compatible with the nominal LCLS design parameters. This having been said, it is important to examine the potential of the LCLS, in terms of flexibility for future developments and to improve the already remarkable qualities of the source. This study, hopefully, will also provide useful input for the exploration and design of future scientific experiments using the LCLS facility.

In the reference design, the bunch is compressed with a two-stage bunch compression system using magnetic chicanes. Bunch compression is achieved by establishing an energy-position correlation within the bunch and transporting this beam through a bend system (e.g., chicane) with an inherent energy-dependent path length. The first bunch compressor, using a magnetic chicane at 250 MeV, shortens the bunch from 0.7 to 0.3 mm (rms). The second compressor, using a double magnetic chicane design at 4.54 GeV, compresses the bunch to its final nominal rms value of 24 μm (255 fs FWHM). The rationale for the choice of two compressors and the choice of parameters is contained in the Design Report. The reference pulse length of 255 fs is derived from the need to obtain peak currents greater than 3.4 kA needed for the SASE FEL process to saturate, given the expected emittance, momentum spread and undulator length. In the course of the study described in this report, analyses are made to shorten the FEL pulse by using

- Stronger magnetic compression of the electron bunch
- Optical compression of the photon bunch
- Optical slicing of the photon bunch
- A combination of the above three methods

The stronger compression of the electron bunch is achieved by increasing the momentum spread along the bunch, increasing the strength of the magnetic field of the compressors or a combination of the two. Although conceptually simple, the task is in fact a difficult one, mostly because of the effect of the emission of coherent synchrotron radiation that becomes more severe as the bunch gets shorter. On the positive side, it appears that the nominal LCLS design has the flexibility and tuning range to test ideas and conduct R&D as outlined in this report.

Optical compression of the photon bunch is obtained by increasing the momentum spread of the electron beam thereby dispersing the photon beam in energy and recombining the photon pulse with a system of mirrors. Similarly to what is done with the electron bunch, this method exploits a difference in the path length, this time of the photons. A very short FEL pulse can also conceptually be achieved by slicing the pulse. It is suggested to do this by again spreading the photon beam in energy and letting a small part of the pulse through an energy collimating slit.

Finally, the potential performance of a hybrid system is explored, where the electron bunch is pre-compressed magnetically to 130 fs (half of its reference length) and the optical pulse is either compressed or sliced.

This report does not consider significant modifications to the LCLS design, such as starting with even shorter bunches from the RF photoinjector. It also appears feasible to mistune the bunch compression so that only a small part of the electron bunch has sufficient phase space density to lase. This is not considered a reliable technique because the stability of such a method is not well understood.

3. Electron Beam Manipulations

3.1 Introduction

The nominal LCLS design [1,2] produces a 24-μm rms electron bunch length (or 255 fsec FWHM) at 14.3 GeV. In this case, if the full bunch enters into SASE saturation, the x-ray pulse will have a similar length. As noted in Section 2, further reduction of the x-ray

pulse length can be achieved by using more electron bunch compression, x-ray pulse compression facilitated by linear energy chirp within the electron bunch, or a combination of these two approaches.

All of these approaches require additional manipulations of the electron beam phase space in the linac, and each scenario adds significant technical risk to the preservation of the electron beam phase space density and also pushes various pulse-to-pulse component stability tolerances. In this section the nominal compression scheme is reviewed first to highlight a few of the design criteria and limitations. Then the possible electron bunch manipulations needed for further compression of the optical pulse are investigated.

3.2 Review of Nominal LCLS Compression

The nominal LCLS accelerator design provides a very narrow electron relative energy spread at 14.3 GeV of <0.03 % rms. This is achieved by using the strong longitudinal geometric wakefields of the micro-bunch in the linac accelerating structures to cancel the correlated energy spread of the second bunch compressor chicanes (BC2). Fig. 3.1 shows the nominal energy-position (or δ-z, corresponding to energy-time) correlation (see lower right plot) immediately after the BC2 chicane at 4.5 GeV [2], but still some 600 meters before the undulator. The bunch is still 'under-compressed' such that the pseudo phase space rotation is <90°. After this point, the beam is accelerated to 14.3 GeV through 560 meters of RF structures (*i.e.* the L3-linac). At 1-nC of charge, and with the 24-μm rms bunch length, a strong longitudinal wakefield is generated in the structures, where the head of the bunch (left side of plots) loads the tail. This loading is very nearly linear along the bunch (for a uniform temporal distribution as in Fig. 3.1) and is used to cancel the correlated energy spread. Fig. 3.2 shows the same plots as Fig. 3.1, but now taken at 14.3 GeV, after the L3-linac. The linear relative energy spread has been reduced by the energy increase, and in addition, it is virtually removed by the L3 wakefield to a level of <0.03 % rms. Table 3.1 lists the critical compression parameters for the nominal case.

Table 3.1. Compression parameters for the nominal design.

Bunch charge	Q	1.0	nC
Initial bunch length from injector (rms)	σ_{z_0}	0.71	mm
RF phase in L1-linac (0° is on-crest)	φ_{L1}	41.0	deg
Momentum compaction of 1st compressor	R_{56} (BC1)	30.6	mm
RF phase in L2-linac (0° is on-crest)	φ_{L2}	34.0	deg
Momentum compaction of 2nd compressor	R_{56} (BC2)	30.4	mm

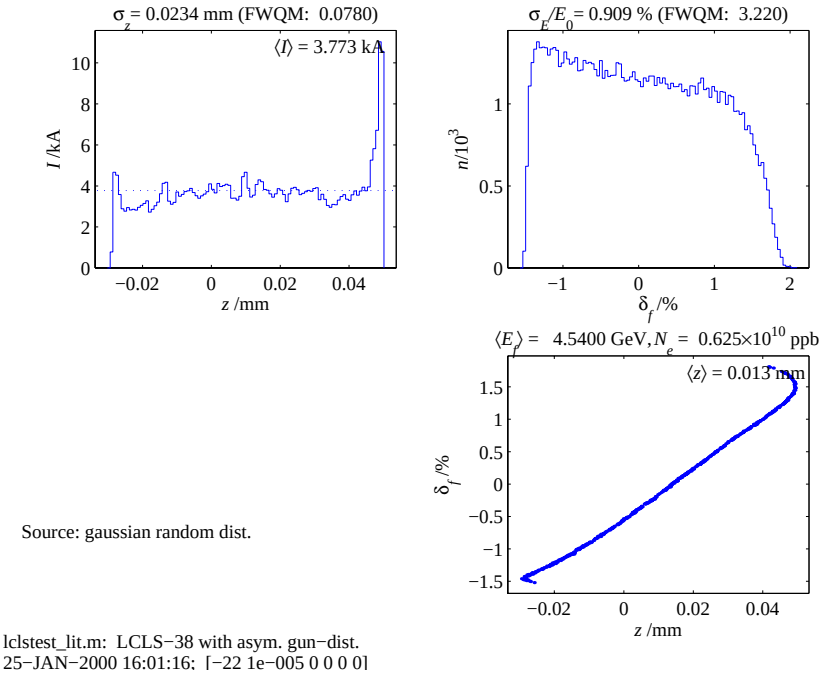

Fig. 3.1. Nominal e^- bunch temporal distribution (top-left), energy distribution (top-right) and longitudinal phase space (lower-right) at 4.5 GeV immediately after the BC2 chicanes but still prior to the L3-linac (bunch head at left toward $z < 0$). The rms energy spread at the BC2 exit, prior to the L3-linac, is 0.9 %.

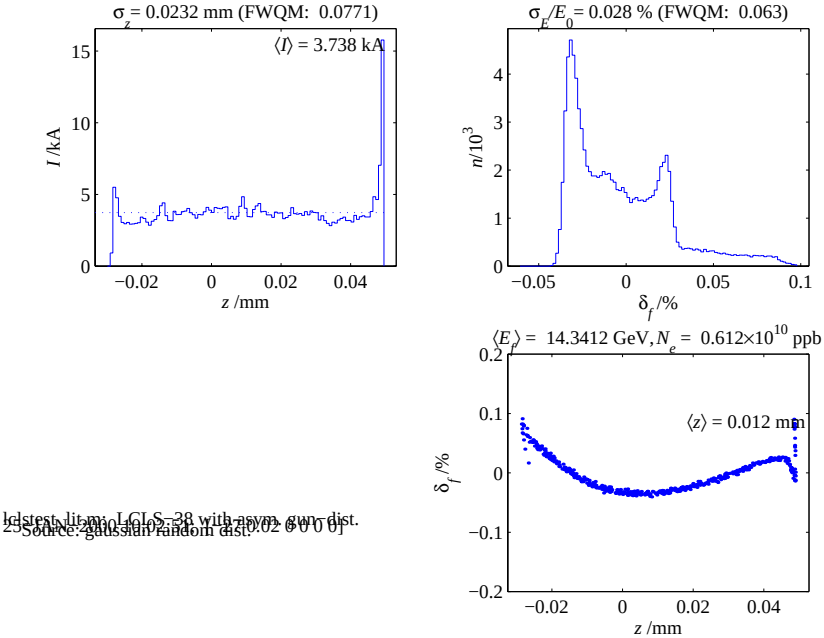

Fig. 3.2. Same *nominal* e^- plots as in Fig. 3.1, but taken at 14.3 GeV, after the L3-linac (*i.e.* just prior to the undulator). The energy spread has been greatly reduced at this point by acceleration and the L3-linac wakefields. The rms energy spread is 0.028 % at 14.3 GeV.

3.3 Scenarios for a Shorter X-Ray Pulse

Four different scenarios are described here which attempt to facilitate a shorter x-ray pulse. Table 3.2 summarizes the four possibilities, including a qualitative description of the phase space dilution 'risk' associated with coherent synchrotron radiation (CSR) and other short-bunch wakefield effects. In all cases the compression parameters of the accelerator need to be adjusted. This is done here in an operational sense, such that no re-design is required. Only magnet power supplies, gun charge, and RF phases and amplitudes are adjusted. Note that the shortest electron bunch length (case-1) is significantly shorter that the 50 fs FWHM "desired" pulse width. The reasons why this cannot be easily "tuned" are discussed in Section 3.3.1.

Table 3.2. Various scenarios which might be used to produce a shorter x-ray pulse. (* positive energy spread implies that the head of the bunch has lower energy than the tail.

scenario	Charge [nC]	e^- FWHM bunch length [fs]	e^- FWHM energy spread [%]*	CSR and wakefield 'risk'
Nominal	1	255	0.06	Nominal
case-1	0.2	10	0.07	High
case-2	1	130	–0.20	High
case-3	1	670	+0.25	Low
case-4	1	255	–2.00	High

3.3.1 Case-1: An Extremely Short Electron Bunch

It might be possible to adjust the second compressor chicane magnets to a slightly stronger setting in order to fully compress the electron bunch. This is an extreme case where the bunch reaches a full-width of just 10 fs while the final energy spread is still just 0.07 %. Figure 3.3 shows the longitudinal phase space in this case-1 where the gun charge has also been reduced to 0.2 nC.

This case generates an extremely short bunch in the second bunch compressor chicane and it may be extremely difficult to preserve the transverse phase space density against the effects of coherent synchrotron radiation (CSR). To mitigate these effects, the total bunch charge in this case has been reduced from 1.0 nC to 0.2 nC and the compression parameters have been re-optimized. The calculations of the CSR effects are extremely subtle in this case and there is presently very limited confidence that, for this extremely short bunch, the effects can be reliably calculated at present. The new compression

parameters are given here in Table 3.3. Note the bunch length at the gun is assumed to be significantly shorter due to the low charge.

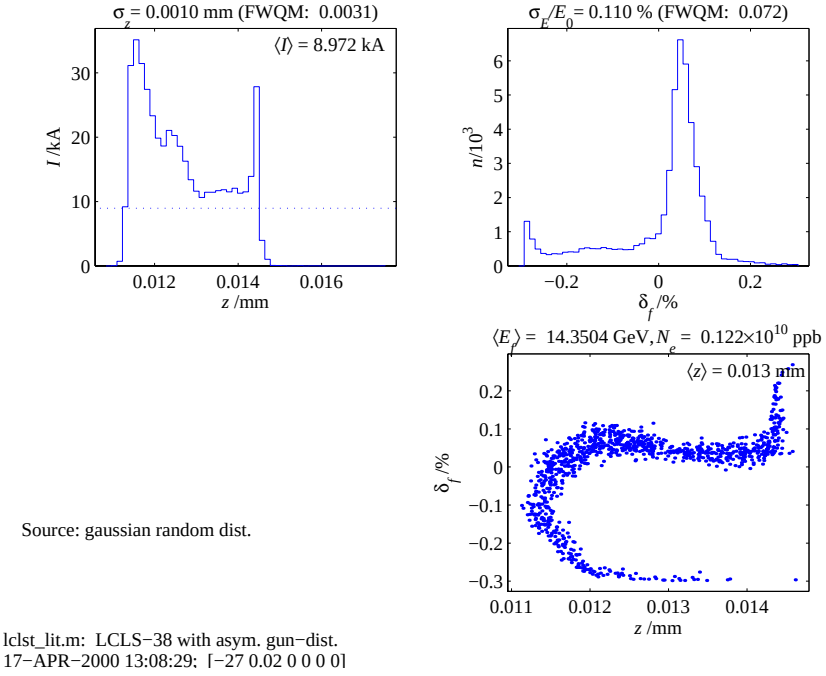

Fig. 3.3. Case-1: An extremely short electron bunch length produced by a lower bunch charge from the gun, and by re-tuning some of the compression parameters.

Table 3.3. Compression parameters for case-1.

Bunch charge	Q	0.20	nC
Initial bunch length from injector (rms)	σ_{z_0}	0.40	mm
RF phase in L1-linac (0˚ is on-crest)	φ_{L1}	48.0	deg
Momentum compaction of 1st compressor	R_{56} (BC1)	30.0	mm
RF phase in L2-linac (0˚ is on-crest)	φ_{L2}	34.0	deg
Momentum compaction of 2nd compressor	R_{56} (BC2)	28.0	mm

It is difficult to 'back-off' on the compression to produce a bunch length of 50 fs, because the bunch continues to display a very narrow, high peak-current area at the head of the distribution (left) in all cases with a total bunch length of <100 fs.

3.3.2 Case-2: A Shorter Electron Bunch with an Energy Chirp

Another method to reduce the length of the x-ray pulse might be implemented by a combination of more electron compression and some final added optical compression. In

this scenario the L2-linac RF phase is moved closer to crest (by 1˚) and the BC2 chicane magnets are increased in field (by ~5 %), still using under-compression. The wakefield induced energy spread of the L3-linac then dominates the final energy spread because of the shorter bunch in L3 (stronger wakefield) and because of the reduced initial energy spread from the re-phased L2-linac. If the bunch is compressed to 12 μm (rather than the nominal 24 μm) the final correlated energy spread after the L3-linac will be 0.22 % full-width, with the bunch head at higher energy than the tail (a negative chirp; see Fig. 3.4). The chirp is quite small, and it is limited again by CSR effects in the compressors, but the combination of electron and x-ray compression might be a practical alternative. Since here the electron bunch does not pass through the singularity point of full compression, the effects of CSR might be more confidently predicted, and the double chicane might be re-optimized to maintain some of the cancellation of the CSR-induced emittance dilution. The RF phase stability tolerances will, however, be even tighter here (<0.05˚ S-band) than in the nominal design in order to keep the peak current in the undulator relatively constant from pulse to pulse.

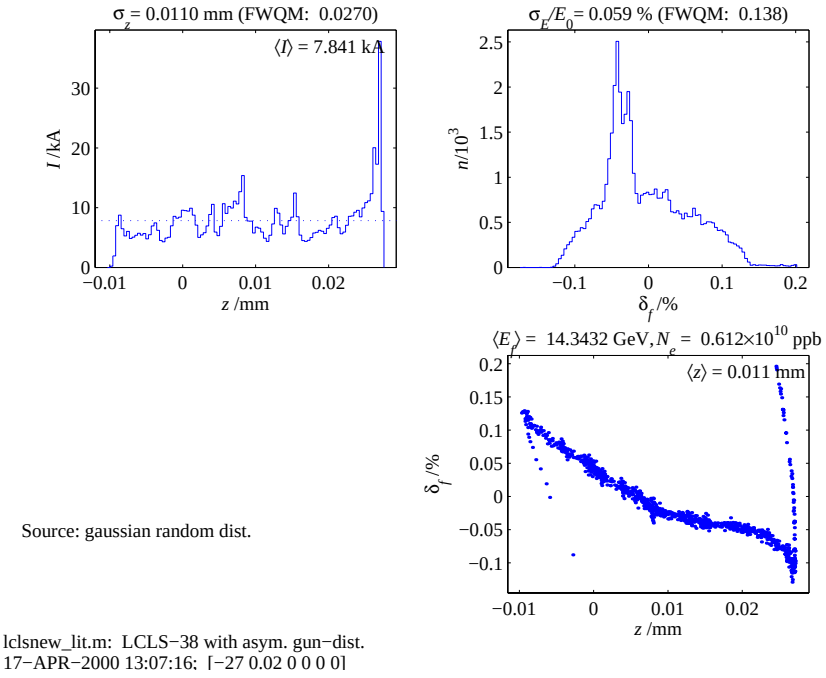

Fig. 3.4. Case-2: A reduced electron bunch length and an accompanying negative energy chirp to facilitate x-ray pulse compression.

Table 3.4. Compression parameters for case-2.

Bunch charge	Q	1.0	nC
Initial bunch length from injector (rms)	σ_{z_0}	0.71	mm
RF phase in L1-linac (0˚ is on-crest)	φ_{L1}	41.0	deg
Momentum compaction of 1st compressor	R_{56} (BC1)	30.7	mm
RF phase in L2-linac (0˚ is on-crest)	φ_{L2}	33.0	deg
Momentum compaction of 2nd compressor	R_{56} (BC2)	33.4	mm

3.3.3 Case-3: A Longer Electron Bunch with an Energy Chirp

A third scenario involves increasing the electron bunch length in order to generate an energy chirp. Since the L3-linac wakefield is reduced with a longer bunch, a chirp can easily be introduced by moving farther off RF crest in the L2-linac which generates a longer bunch and leaves more correlated and uncompensated energy spread. Here the bunch head is at lower energy than the tail (a positive chirp; see Fig. 3.5). The small chirp might then be used to compress the x-ray pulse. The risk of phase space dilution in this case is even lower than that of the nominal case. This advantage (i.e. ease of electron setup) must be balanced by the difficulties of optical compression from 670 down to 50 fs with a small (0.25% full-width) energy spread.

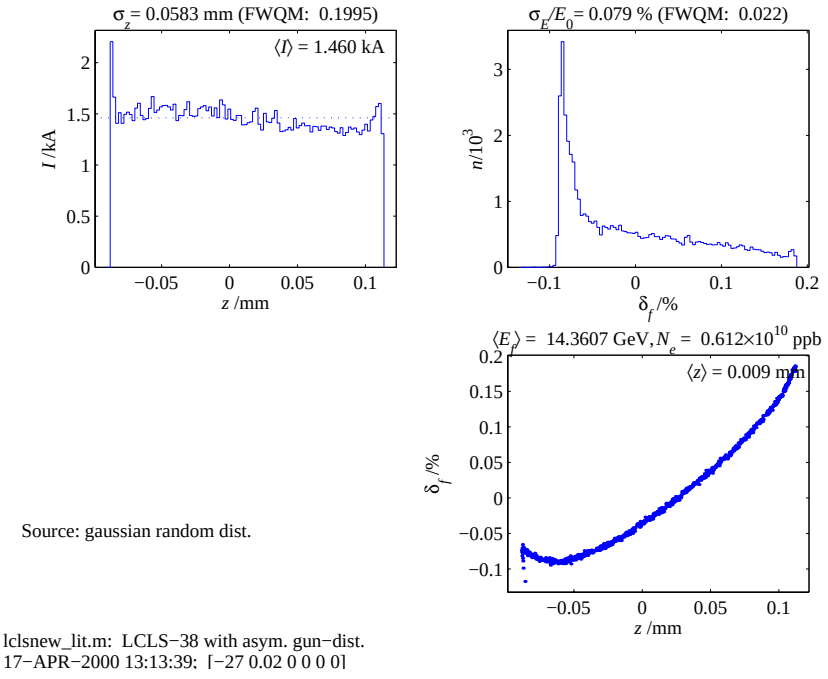

Fig. 3.5. Case-3: An *increased* electron bunch length and an accompanying positive energy chirp.

Table 3.5. Compression parameters for case-3.

Bunch charge	Q	1.0	nC
Initial bunch length from injector (rms)	σ_{z_0}	0.71	mm
RF phase in L1-linac (0° is on-crest)	φ_{L1}	41.0	deg
Momentum compaction of 1st compressor	R_{56} (BC1)	30.7	mm
RF phase in L2-linac (0° is on-crest)	φ_{L2}	36.0	deg
Momentum compaction of 2nd compressor	R_{56} (BC2)	24.0	mm

3.3.4 Case-4: An Energy Chirp with no Change in Final e^- Bunch Length

This case considers the possibility of achieving a much larger final correlated energy spread. Note that the linear correlation at BC2 (in Fig. 3.1) is introduced by off-crest RF phasing (41°) in the L2-linac before BC2. The positive sign in the Fig. 3.1 correlation ($\langle z\delta \rangle > 0$, with bunch head toward $z < 0$) is required so that the bunch length is *compressed* (rather than expanded) in the BC2 chicanes. This sign cannot be arbitrarily reversed unless a more complicated compressor design (that includes quadrupole magnets) is substituted for the chicanes. This means that for a chicane-type compressor (desired for its simplicity and adjustability) the wakefield in the L3-linac always generates a correlation which is opposite in sign to the correlation needed for bunch compression. This cancellation greatly aids in the *nominal* machine design, but also makes it difficult to provide more than ~0.1 % rms linear energy spread ('chirp') by re-phasing the L2-linac. Moving farther off-crest quickly reduces the L2-linac energy gain, without generating a significant energy chirp. Moving closer to RF crest generates more compression-limiting RF non-linearity and also forces a stronger chicane, which risks significant bend-plane emittance dilution due to CSR, again with only a minor energy chirp generated.

Similarly, generating a chirp by off-crest phasing in the L3-linac is not practical. This is due to the very short bunch in L3 (24-μm rms) and the relatively long RF wavelength in the SLAC linac ($\lambda \approx 10.5$ cm). The rms relative energy spread, σ_δ, generated by an off-crest accelerating voltage of $eV = GL$, for an rms bunch length of σ_z is given by

$$\sigma_\delta \approx \frac{2\pi\sigma_z}{\lambda E_f} GL \sin\varphi \ ,$$

where E_f is the final beam energy (~14 GeV), G is the accelerating gradient (~19 MeV/m), L is the linac length (~560 m), and φ is the RF phase ($\varphi = 0$: on-crest). Even for a 45° RF phase (which would mean the L3-linac accelerating gradient would somehow need to be increased by $\sqrt{2}$ in order still to achieve 14 GeV) a 24-μm rms bunch will only generate 0.08 % rms energy spread at 14 GeV. Therefore, generating a significant chirp in the S-band L3-linac using only RF phasing is impossible.

Excluding a complete re-design of the compression systems, this leaves one possibility: 'over-compression'. Bunch compression in BC2 is nominally configured as 'under-compression'. This is the condition when the 'rotation' in longitudinal phase space is less than $\pi/2$. In this case a positive $\langle z\delta \rangle$ correlation prior to the chicane remains positive after the chicane. This is a desirable configuration since it requires a weaker chicane than does over-compression and, more importantly, does not cross over the $\pi/2$ rotation point somewhere inside the chicane. This cross-over point (*i.e.* 'full-compression') is associated with an extremely short bunch of just a few microns in the case of the LCLS. If this point occurs in the middle of a bending system, the strong CSR and potential wakefields of the very short bunch might be very damaging to the bend-plane emittance. If these effects are not too severe [4], however, over-compression offers much greater potential for generating significant electron chirp prior to the undulator.

Ignoring the emittance growth effects described above, over-compression of the LCLS bunch in BC2 is quite easy. If the nominal BC2 chicane dipole fields are simply increased 9.5 %, the bunch will over-compress, as shown in Fig. 3.4, with a final negative $\langle z\delta \rangle$ correlation immediately after the chicanes. This arrangement produces the same bunch length [5] as does under-compression, yet with a negative $\langle z\delta \rangle$ correlation. The acceleration in the L3-linac to 14 GeV will now generate nearly the same wakefield as before, which will now *add*, rather than cancel, the net $\langle z\delta \rangle$ correlation, making it even more negative. Fig. 3.6 shows the same plots as in Fig. 3.2, but now calculated for the case of over-compression. In this case, the full-width energy spread is 2 % at 14.3 GeV and has a negative, and nearly linear, $\langle z\delta \rangle$ correlation. The rms bunch length, after the DL2-bend system, is back to the nominal value of 24 μm. The bunch charge remains at 1 nC. This figure shows that the leading electrons (the bunch head at $z < 0$) are now at higher energy than the trailing electrons. This correlation should generate an accompanying optical chirp that might be used to compress the x-ray pulse to below 50 fsec. This level of chirp (~2 % FWHM) cannot be generated with a positive $\langle z\delta \rangle$ correlation (*i.e.* using under-compression).

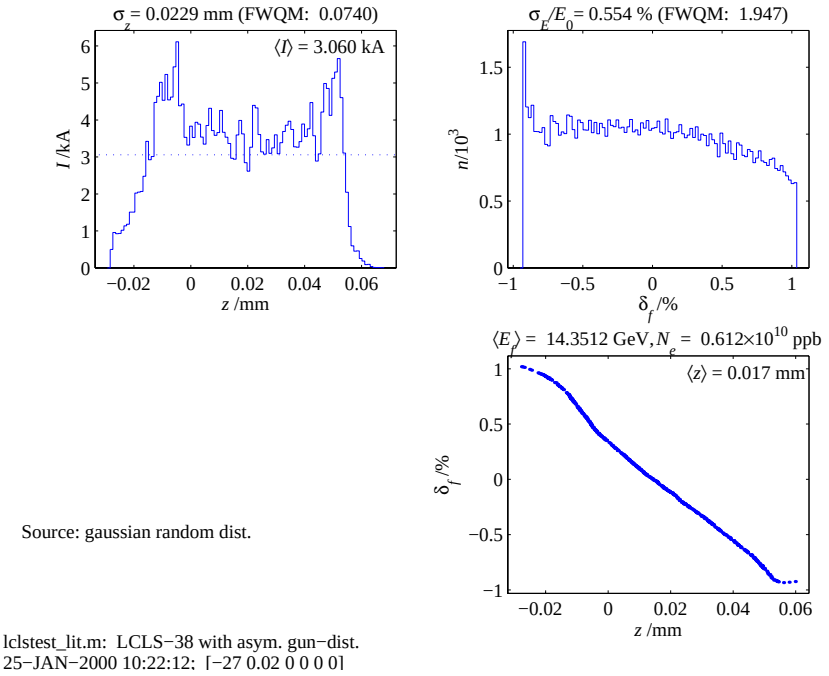

Fig. 3.6. Same plots as Fig. 3.2 (at 14 GeV, after the L3-linac and just prior to the undulator), but shown for over-compression. The negative chirp has a full-width energy spread of 2 % (bunch head energy higher than tail) and the rms bunch length, after the DL2-bend system, is 23 μm.

Table 3.6. Compression parameters for case-4.

Bunch charge	Q	1.0	nC
Initial bunch length from injector (rms)	σ_{z_0}	0.71	mm
RF phase in L1-linac (0˚ is on-crest)	φ_{L1}	41.0	deg
Momentum compaction of 1st compressor	R_{56} (BC1)	30.7	mm
RF phase in L2-linac (0˚ is on-crest)	φ_{L2}	38.0	deg
Momentum compaction of 2nd compressor	R_{56} (BC2)	30.4	mm

3.4 Roughness Wakefields

The short bunch can also generate longitudinal wakefields in the undulator vacuum chamber due to surface roughness effects. The wakefield can generate energy spread and energy loss within the undulator which may drive parts of the bunch far enough off energy to significantly reduce the FEL gain. Present estimates allow for only 0.1 % rms energy spread generated *within* the undulator. In addition, a net energy loss might drive the full bunch off resonance if the magnetic fields in the undulator are not tapered at the right level along the length of the undulator. The loss tolerance is similarly estimated at <0.1 %.

Previous analysis of the surface roughness impedance [6,7] assumed that the bunch length was larger than the typical size of the roughness bumps on the wall. In this case, the theory predicts that the longitudinal impedance due to the roughness is purely inductive. For very short bunches, this assumption is not valid any more, and a modification of the theory is necessary [8]. Here we present the main results of the modified theory applicable for very short bunches. In the limit of high frequencies, the impedance has both inductive and resistive components.

To simplify calculations, we consider a model in which the wall roughness is represented by a sinusoidal perturbation of the pipe wall, with amplitude h and wavelength λ, so that the pipe radius $r(z)$ is given by

$$r(z) = b + h\sin\frac{2\pi z}{\lambda},$$

with the amplitude of the corrugations much smaller than the wavelength, $h << \lambda$. In this case the wake for a point charge, per unit length of undulator, is

$$w(s) = \frac{1}{2\sqrt{\pi}}\frac{h^2 L\kappa^{3/2}}{b}\frac{\partial}{\partial s}\frac{1}{\sqrt{s}}\left(\cos\frac{\kappa s}{2} + \sin\frac{\kappa s}{2}\right)$$

where $\kappa = 2\pi/\lambda$.

Using this equation the wakes, accumulated over the length of the undulator L, for different bunches, corresponding to the nominal case, case-1 and case-2 are calculated. In these calculations, a flat profile for the bunch distribution is assumed. The parameters used in those calculations are: number of particle $N = 6\cdot10^9$ (1 nC) for both the nominal case and case-2, and $N = 1.2\cdot10^9$ (0.2 nC) for case-1, the roughness amplitude $h = 0.28\ \mu$m (corresponding to the RMS roughness of $0.2\ \mu$m), the wavelength $\lambda = 100\ \mu$m, the undulator length $L = 100$ m, the beam energy in the undulator $E = 15$ GeV, and the pipe radius $b = 2.5$ mm. The roughness parameters are chosen in agreement with the roughness measurements described in Ref. [9]. The figures below show the relative energy gradient developed across the bunch after the passage of the full undulator length. The 10-fsec case (case-1) is marginal, while the other cases shown here appear to meet the required specifications.

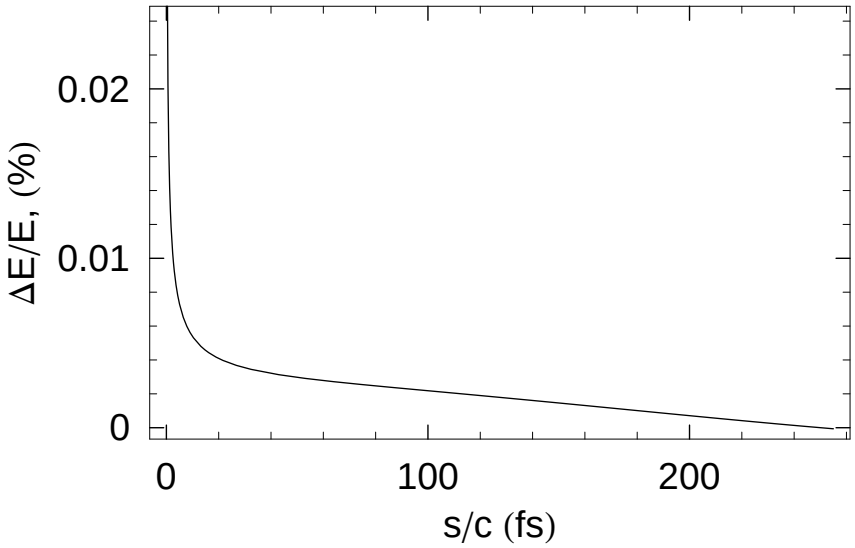

Fig. 3.7 Relative energy variation with the bunch for the nominal case (bunch length is 255 fsec FW). The average energy loss is 0.0021 %.

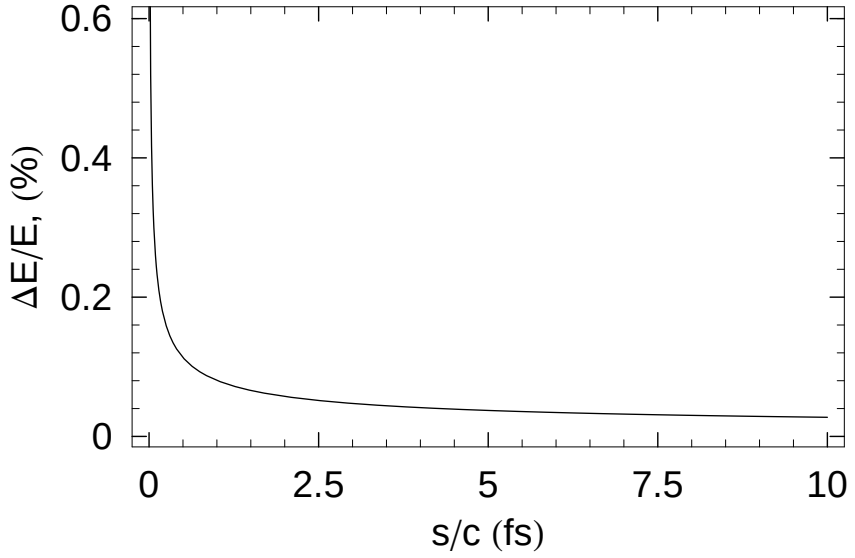

Fig. 3.8 Relative energy variation with the bunch for case-1 (bunch length is 10 fsec FW). The average energy loss is 0.05 %.

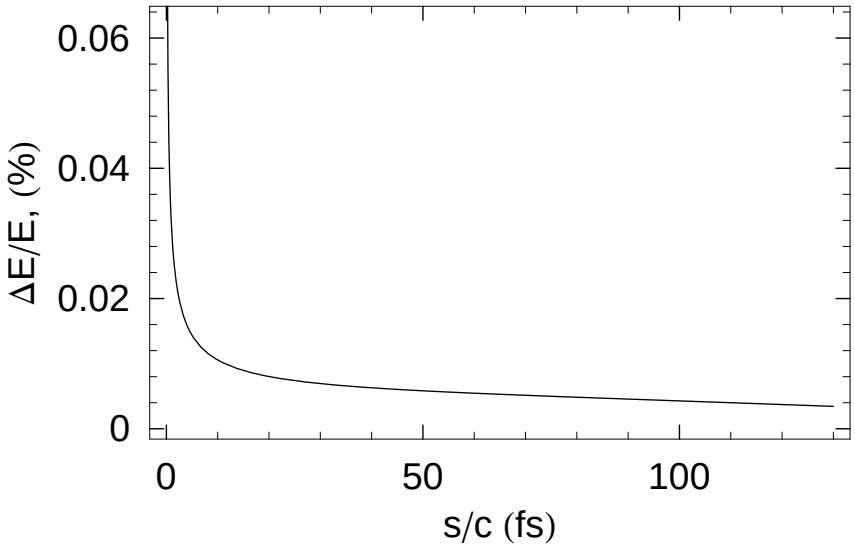

Fig. 3.9 Relative energy variation with the bunch for case-2 (bunch length is 130 fsec FW). The average energy loss is 0.0065 %.

4. Optical Pulse Compression and Slicing Techniques

4.1 Overview

There are in principle numerous ways to approach the problem of slicing or compressing a radiation pulse. From a general point of view these can be associated with the modulation of the pulse's parameters in any of its six phase space dimensions. A usual approach is to induce a time or distance correlated "chirp" in one of the dimensions and then pass the pulse through an aperture (for slicing) or a medium with dispersion (for compression) along the conjugate dimension. In some instances, the initial chirp may be transformed into a chirp in an alternative phase space dimension (or dimensions) prior to the aperturing or dispersion operation. From this perspective it is also useful to note that even an ordinary operation such as, e.g., focusing can be viewed as the direct application of dispersion within an individual phase space dimension.

For the LCLS, the initial correlated modulation is confined (nominally) to longitudinal phase space (see Section 3), specifically to the pulse energy. Both pulse slicing and compression techniques based on aperturing or dispersion in both longitudinal and transverse phase spaces have been investigated. A selected set of techniques that have been emphasized in preparation for the pending LCLS CDR is depicted in Fig. 4.1.

On the top left, pulse slicing is achieved by passing the radiation pulse through a diffractive optic which converts the energy chirp into an angular chirp [10,11,12]. The optic

is designed to both disperse and focus the pulse segments of different energy onto the vicinity of its symmetry axis. The approximate focal waist of the angularly swept beam passes over a fixed aperture which executes the slicing action. On the top right, a slicing technique based on the insertion of an energy aperture directly into the longitudinal phase space of the pulse is shown. In this case the aperture is an ordinary multilayer, with parameters optimized for maximal efficiency. The chopping mechanism is the selective reflection of only that sub-interval of the pulse that fulfills the multilayer Bragg condition [13,14]. On the bottom left a compression scheme based on the use of double gratings is schematized. The energy chirp is converted into an angular chirp by a reflection grating and the angle-dependent path length (or distance) dispersion is converted into a longitudinal compression by the second grating [15,16]. On the bottom right a hybrid compression technique based on a single grating followed by an array of mirrors is drawn. As in the double-grating scheme, the first optic transforms the energy chirp into an angular chirp. This chirp is then converted into a longitudinal compression, along with simultaneous transverse focusing, by the specially configured array of curviform mirrors [17].

In the subsequent sections the expected performance of each of these techniques for LCLS radiation pulse parameters corresponding to the cases tabulated in Table 3.2 will be discussed

4.2 Transmission Grating & Zone Plate Based Slicing Techniques

First a simple analytical model [11,12] of the slice duration in terms of the zone plate and energy chirp parameters is used to evaluate the energy chirp scenarios and select zone plate parameters.

$$\tau_{slice} = a \cdot \frac{\lambda_0 \cdot z_{image} \cdot T \cdot \delta}{D \cdot \Delta \cdot \left(\lambda_0 \cdot z_{image} + \delta^2 - \delta \cdot D\right)} \cdot$$

This equation gives the minimum duration, τ_{slice} (FWHM), of the time slice expected from a portion of an off-axis zone plate with minimum feature size δ, and aperture D, as a function of zone plate image distance z_{image}, for given values of the pulse duration T, and photon chirp half width Δ. The constant *a* is approximately equal to 1.

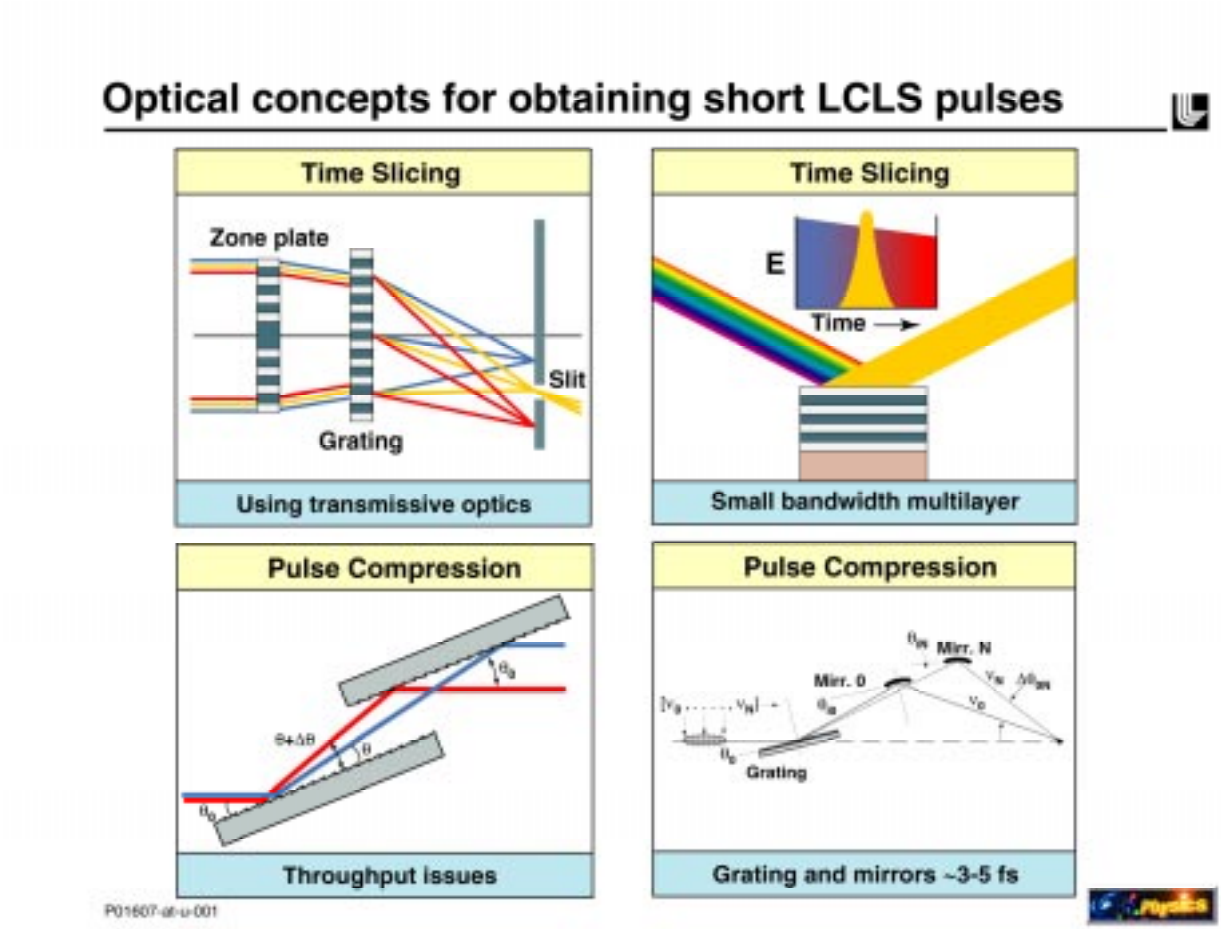

Figure 4.1. Radiation pulse slicing (top) and compression (bottom) techniques for the LCLS.

The time-slicing performance of a plausible sputtered-sliced off axis zone plate, one that has a minimum feature size of $\delta = 0.35 \cdot \mu m$ and a total aperture of D=200μm is now considered. This lens has a fairly large aperture and small feature size, and although technically challenging, probably represents what is practical for the manufacture of a sputtered-sliced zone plate. Fig. 4.2 shows a plot of the time slice (FWHM) vs. image distance for this off-axis zone plate for the 3 energy chirp scenarios (all the electron bunch scenarios and cases in this section are listed in Table 3.2). In general the slice time decreases with increasing focal length but approaches

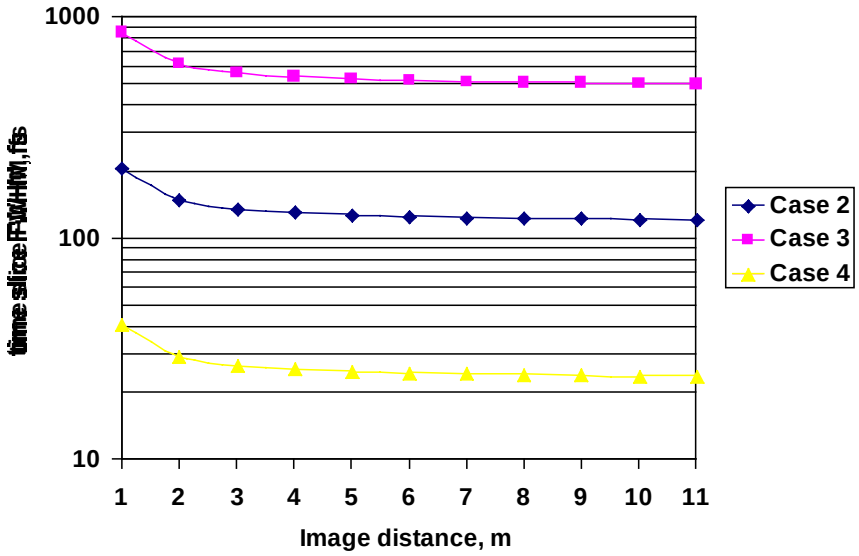

Figure 4.2. Time slice duration vs. image distance for a zone plate in an off-axis geometry. Zone plate aperture D = 200μm; minimum feature size δ = 0.33μm.

a limiting value for focal lengths over 4 meters. In cases 2 and 3, the speed of the spot is so small that barely moves a distance equal to its spot size over the full duration of the pulse. This lens will not produce a time-sliced FEL pulse under energy chirp scenarios 2 and 3. Case 4, however, does produce a reduced pulse duration of just over 40 fs with a 1 meter focal length and asymptotically approaches a value of just above 20 fs. Although the slice duration gets smaller by several fs from 3 to 5 meters this must be traded against the decrease in the power density in the focal spot with increasing focal length.

Next an assessment of the slit plane focal density attainable for the LCLS with n diffractive elements used in sequence and focusing in d dimensions is considered. A linear zone plate that focuses in 1 dimension will *increase* the central photon density by the ratio of the σ of the unfocused beam to the σ of the focused spot. If focusing is achieved in both dimensions, with a circular zone plate or with crossed X and Y linear zone plates, the photon density will increase by this ratio squared. At the same time the photon density will be *decreased* by the efficiency of the lens ε, or by ε^2 for two lenses, as well as the loss of beam due to the finite aperture of the system. Using the diffraction limited spot size derived above for a focusing optic of aperture D, the central photon density of the focused spot integrated over a slice time τ_{slice} will be:

$$\rho_{slice} = \frac{\varepsilon^n P_{sat}}{2\pi E_p \sigma_{beam}^2} \cdot \left(\frac{2\sqrt{2\ln(2)}\,\sigma_{beam} D}{a\lambda_0 z} \right)^d \cdot \left(\frac{1}{\sqrt{2\pi}\sigma_{beam}} \int_{-D/2}^{D/2} e^{\left(-\frac{1}{2}\frac{x^2}{\sigma_{beam}^2} \right)} dx \right)^2 \tau_{slice}$$

where *n* is the number of lenses, *d* is the number of focused dimensions and the integral is the aperture efficiency factor. This function gives the cumulative photon density produced by a system of off-axes zone plates at a fixed point in space integrated over the duration of the time slice. The photon density is linearly proportional to the FEL saturated power level, P_{sat}, and slice duration, τ_{slice}.

Under this assumption three separate optical systems are considered. The first is a single off-axis linear zone plate producing a line focus at the sample in one dimension. The second consists of two off-axis linear zone plates, one focusing in the x direction followed by another focusing in the y direction. This system produces a spot focus at the sample but its intensity is somewhat reduced by the efficiency of the second lens. The third optical system consists of a single off-axis circular zone plate producing a spot focus at the sample. Fig. 4.3 shows the resulting cumulative photon densities for the three optical systems as a function of image distance. The different curves in each plot are for lenses of deferring aperture ranging from 200 μm down to 25 μm.

Both linear and circular transmissive zone plates and linear gratings, operating at 8 keV, have been manufactured in the past at LLNL using the sputter-slice technique [18]. As a result of recent studies of materials energy loading by the LCLS [19], the idea of using very low Z alternating materials (e.g., C/x, B/x, or Be/x) systems for the fabrication of diffractive-transmissive elements has been proposed as a means of reducing the damage threshhold and numerical simulations have affirmed the feasibility of the concept.

4.3 Multilayer Based Slicing Techniques

The interaction of a radiation pulse with any passive periodic structure can in general modulate any of its phase space distributions. For the case of a multilayer interacting with an LCLS pulse, the dominant modulation effect is restricted to the pulse's temporal distribution. This is readily understood by observing that the successive reflection of the pulse off the structure's successive layers leads to a superposition, in the reflected beam, of a sequence of incrementally delayed (and modulated) copies of the input pulse. This results in an effective temporal dilation of the pulse. In order to simulate this effect, the spectral response (complex amplitude reflectivity) of the multilayer must first be calculated.

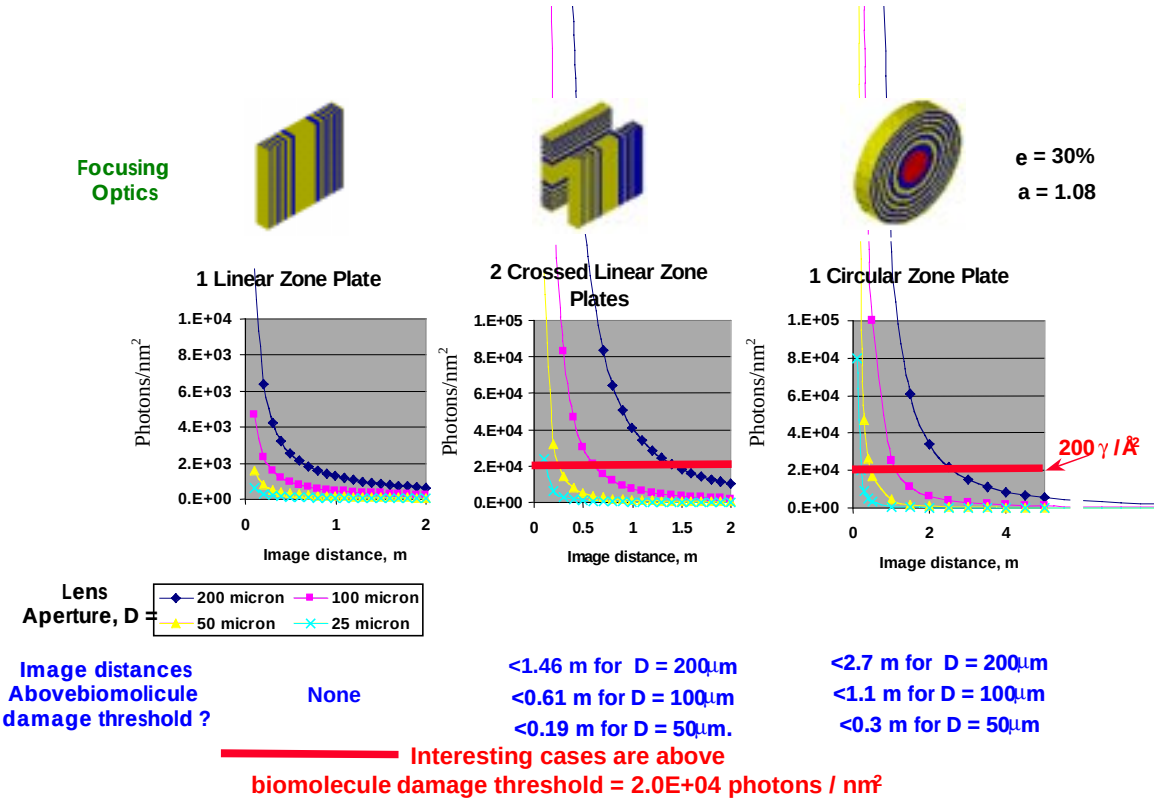

Figure 4.3. Attainable LCLS photon densities for focused 50 fs time-slices using various transmissive diffractive components.

For the case studies reported on here both the multilayer reflectivity responses and the temporal distortion effects on LCLS pulse models were calculated using computer codes developed at SSRL [13,14] and LLNL [14]. The SSRL multilayer code, based on a self-consistent dynamical scattering formalism [20], has been proven in recent years in the study and development of various multilayer structures for X-ray optics applications [21]. Using these codes a series of parameter studies of various multilayer systems were performed to identify material pairs that would provide the narrowest possible bandwidths at acceptable levels of reflectivity. The study results to date indicate that bandwidths ranging from ~1.0 % down to ~0.077% at reflectivities of between ~50% and ~70% can be attained with conventional systems such as W/B_4C, and a broad family of metal/metal-disilicide systems.

The temporal responses of selected multilayers were calculated by computing the Fourier Transform (FT) of the computed amplitude reflectivity functions. Using these, the

temporal response of the multilayers was simulated by convolving the FTs with finite sinusoidal wave trains corresponding to the micro-pulses comprising a typical LCLS pulse. In general, the major effect of the temporal distortion is a dilation of the coherent wave train of each LCLS micropulse (which are typically between 300 and 600 wavelengths long) by up to ~50% of its length. The overall effect on the LCLS pulse is, apart from the attenuation by the multilayer reflectivity, a slight smoothing of the temporal structure

The slicing performance of any of the investigated multilayers can be readily estimated with

$$\tau_{slice} \cong \frac{\sqrt{2\pi}\sigma_{\varepsilon M}}{\Delta E_p / E_p} \times T$$

where T is the total pulse length, τ_{slice} is the length of the pulse slice, ΔE_p is the total energy chirp, E_p is the nominal pulse photon energy, and $\sqrt{2\pi}\sigma_{\varepsilon M}$ is the multilayer bandwidth. In Table 4.1 the slicing performance of a set of selected multilayers for the various cases listed in Table 3.2 is shown. Provided that the corresponding (**Zr/$ZrSi_2$**) multilayer can be fabricated and that, once fabricated, performs in accord with theory, sliced pulse lengths extending down to ~5 fs appear to be attainable.

Table 4.1. Slicing performance of selected multilayers for various cases of electron bunch length compression and induced energy chirp.

	BW [%]	**Case 1** Δτ	**Case 2** Δτ	**Case 3** Δτ	**Case 4** Δτ
W/B_4C	**0.5**	N/A	N/A	N/A	**32 fs**
Mo/$MoSi_2$	**0.17**	N/A	**~55 fs**	**~228 fs**	**~11 fs**
Zr/$ZrSi_2$	**0.077**	N/A	**~25 fs**	**~103 fs**	**~5 fs**

An important extension of the basic planar multilayer slicer is to the combined slicing and focusing of LCLS beams. Recent advances in techniques for multilayer deposition on curved surfaces [22], combined with the fabrication of extremely high quality curved surfaces [23,24] allows the consideration of optics for demagnifying the LCLS source beam by factors of perhaps as much as ~5000. Using photons/$Å^2$ delivered to the focal waist as a figure of merit [25], the performance figures of a set of ellipsoidal reflectors coated with the multilayers of Table 4.1 are listed in Table 4.2. The radiation pulse parameters correspond to "Case 4" of Table 4.1.

Table 4.2. Focal plane LCLS photon densities achievable with multilayer-coated ellipsoidal focusing/time slicing reflectors. Nominal density in the raw LCLS beam ~ 1 ph/ Å^2

f [cm]	L [m]	Focal Waist [Angstroms]	W/B_4C [photons/ Å^2]	Mo/$MoSi_2$ [photons/ Å^2]	Zr/$ZrSi_2$ [photons/ Å^2]
50	50	10000	1.25×10^3	430	196
25	50	5000	5×10^3	1.72×10^3	784
10	50	2000	3.1×10^4	1.08×10^4	4.9×10^3
2	50	400	7.8×10^5	2.69×10^5	1.23×10^5
1	50	200	3.13×10^6	1.08×10^6	4.9×10^5

This class of optics has the important property that the phase front of the focused pulse remains isochronic, which, apart from the relatively small smoothing induced by the multilayer, preserves the temporal structure of the source.

4.4 Reflection grating based compression techniques

4.4.1 Reflection grating pair (2-grating compressor)

In this section we discuss the characteristics of the two-grating compressor shown in the bottom left of Fig. 4.1 [15]. The incidence angle θ_0, is assumed to be very small compared to 1, but large compared to the angular spread in the radiation beam. The grating period is a, and the two gratings are displaced in the direction normal to their surfaces by D, and in the direction parallel to their surfaces by L. The waist of the beam impinging on the first grating is denoted by w and of the one diffracting off the second grating by W. The footprint length of the diffracted beam on the second grating is denoted by δ. For the present discussion let the diffraction angles corresponding to the two extremal energies in the chirped beam be θ and $\theta+\Delta\theta$. In this case the following relations apply (for $\theta_0 << \theta << 1$ and diffraction broadening effects disregarded):

$$\theta \cong \sqrt{\frac{2\lambda}{a} - \theta_0^{\,2}}; \frac{\Delta\theta}{\theta} \cong \frac{\Delta E_p}{E_p}; L \cong \frac{D}{\theta}; \delta \cong L\left(\frac{\Delta E_p}{E_p}\right); W \cong \delta\theta_0$$

The resulting path length difference between the extremal paths, which usually will be assumed to be equal to some sub-interval of the LCLS pulse length cT, is given by

$$\Delta path \cong D\,\theta\,\frac{\Delta E_p}{E_p}$$

Here a primary constraint is that the diffraction angles θ_0, θ, and $\Delta\theta$ be small enough to ensure adequate throughput efficiency (which is governed by the reflectivity of the gratings), as well as adequate suppression of peak power damage effects at the wavelength of interest. Taking $\theta_0 = 0.0002$ radians and $a = 5\mu m$ with these goals in mind, the approximate compressor parameters listed in Table 4.3 are readily derived for the four cases shown in Table 3.2.

Table 4.3. Two-grating LCLS compressor parameters. λ=1.5Å, w=100μm, Δ_{path}=cT.

	Case 1	**Case 2**	**Case 3**	**Case 4**
Chirp $\Delta E_p/E_p$ [%]	0.14	0.4	-0.5	4
θ [P]	0.0077	0.0077	0.0077	0.0077
D [m]	0.92	0.42	17.4	0.83
L [m]	120.5	55	2260	108
δ [m]	0.169	0.2	11.3	4.3
W [mm]	0.169	0.2	11.3	4.3

Here it is important to note that for the dispersion distances involved effects come into play that can negatively affect the performance of the compressor. The primary one is angular diffraction spread, which, if greater than the wavelength-dependent angular chirp, causes the loss of directional resolution of the diffracted rays of different energies. This spread can be shown to be always greater than the quantity $1/N_g$, where N_g is the number of illuminated grating bars. Using this quantity as a criterion it is evident that there will be negligible compression for Case 1 listed in Table 4.3, marginal compression for Case 2, and no more than ~50% for Case 3. For Case 4 $1/N_g \sim 0.00025\Delta E_p/E_p << 0.0077\Delta E_p/E_p$, indicating a potential lower bound on the compressed pulse of ~8.3 fs. To get a more accurate estimate of the actual performance for Cases 2-4, it will be necessary to analyze the actual diffraction spread more thoroughly.

At the same time it is important to note that the two-grating configuration has the potential advantage of imposing a minimal temporal distortion on the LCLS micropulses, and is thus in principle capable of attaining the greatest degree of compression. A corresponding benefit of this is that one can deliver not only a maximal number of photons to an experiment requiring a short pulse, but the fluctuations inherent in SASE FEL pulses get reduced roughly by the square root of the compression factor. For these reasons, studies are being continued [15] to try to identify alternative grating structures, materials, and configurations with which it might be possible to minimize optical losses and the effects of diffraction spread.

4.4.2 Reflection grating + mirror array

One possible step in this direction is the configuration depicted in the bottom right hand side of Fig. 4.1. Here the grating performs the same dispersive function as the first element of the two-grating scheme. The rays are dispersed in angle space and different groups with different wavelengths get intercepted by independent mirrors, which focus each group of rays onto a common focal area. The positions and attitudes of the mirrors are arranged to provide a total path length difference between the extremal rays which is equal to the LCLS pulse length. In this scheme the grating density can be made large enough to suppress diffraction-spread, i.e., the angular chirp induced by the pulse's energy chirp can be made very much larger than $1/N_g$. This is made possible with the use of multilayer-coated mirrors, which can intercept the dispersed rays at relatively large angles in close proximity to the first grating. Detailed studies of this system with the aim of assessing its performance for the four cases considered in this report are a subject for ongoing and future R&D.

5. Conclusions

This report has investigated a range of design possibilities that may be used to further reduce the x-ray pulse duration in the LCLS from the nominal 255 fs down to 50 fs.

For electron bunch compression, four representative cases were studied to directly compress the bunch further and to partially compress the bunch and/or provide the needed energy chirp to enable x-ray pulse compression. Further analysis is needed to better understand the technical risks associated with the beam manipulations in these cases.

A number of optical schemes for either slicing or compressing LCLS pulses have been reviewed. Although substantial progress has been made in various R&D areas associated with some of the methods, substantial work remains to be done, particularly in the design, fabrication and testing of reflection gratings, multilayers, and transmission-diffraction structures, and in the design and development of actual instruments based on these components. An important area for further analytical and numerical work is also the study of the effects of material and structural imperfections (both systematic and random) on the idealized performance of all the optical schemes.

Although it is too early to decide whether to include these possibilities in the reference design at this time, the LCLS design has been shown flexible enough to enable tuning modifications that allow for the possibility of shorter bunches after the LCLS is commissioned.

References

[1] *LCLS Design Study Report*, SLAC-R-521, Rev. Dec. 1998.

[2] The nominal compression parameters have been modified with respect to reference [1]. The parameters used in this note are those described in LCLS-TN-99-3 (page-3, Table-1), May 3, 1999.

[3] *Workshop on Science and Instrumentation for the Linac Coherent Light Source*, (I.Lindau and J.Arthur, eds.), October 15-16, 1999, SLAC/SSRL, Stanford University.

[4] Detailed and non-trivial calculations need to be done to verify the severity of the effects. Even so, the effects in this 1-μm bunch length regime are quite subtle, and calculations with a satisfactory confidence level may not be achievable at present.

[5] The bunch length just after BC2, for the case of over-compression, has been set slightly larger than for under-compression (30 μm versus 24 μm) because the large chirp at 14 GeV instigates an slight additional compression of 6 μm in the DL2-bend system, which resides immediately upstream of the undulator.

[6] K.L.F. Bane, C.K. Ng, and A.W. Chao, *Estimate of the Impedance due to Wall Surface Roughness*, SLAC-PUB-7514, SLAC, 1997.

[7] G.V. Stupakov, *Impedance of Small Obstacles and Rough Surfaces*, Phys. Rev. ST Accel. Beams, 1:064401, 1998.

[8] G.V. Stupakov, To be published.

[9] Gennady Stupakov, Ruth Ellen Thomson, Dieter Walz, and Roger Carr, *Effects of Beam Tube Roughness on X-Ray FEL Performance*, Phys. Rev. ST Accel. Beams, 2:060701, 1999.

[10] R. Tatchyn, *LCLS Optics: Selected Technological Issues and Scientific Opportunities*, in Proceedings of the Workshop on Scientific Applications of Short Wavelength Coherent Light Sources, W. Spicer, J. Arthur, and H. Winick, eds., SLAC-Report-414, February 1993.

[11] R. Bionta, *A Transmissive Optics Approach for Time-Slicing the LCLS X-Ray Pulse,* LCLS-TN-00-7 (2000).

[12] R. Bionta, *Time-slicing the LCLS FEL with off-axis zone plates*, presented at the LCLS TAC Review, SLAC, 5/19-20/00.

[13] R. Tatchyn, report in progress.

[14] R. Tatchyn, *Multilayer-based Pulse Slicing and Compression*, presented at the LCLS TAC Review, SLAC, 5/19-20/00.

[15] C. Pellegrini, *Radiation Pulse Compression for a SASE-FEL,* LCLS-TN-99-5 (1999).

[16] E. B. Treacy, *Optical Pulse Compression With Diffraction Gratings,* IEEE J. Quant. El. 5(9), 454(1969).

[17] C. Pellegrini, R. Tatchyn, report in progress.

[18] R. M. Bionta, K. M. Skulina, J. Weinberg, *Hard X-ray sputtered-sliced phase zone plates,* Applied Physics Letters 64(8), 945-7, (1994).

[19] R. Bionta, *Controlling Dose to Low Z Solids at LCLS*, LLNL UCRL-ID-137222, January, 3, 2000; LCLS-TN-00-3.

[20] M. Born and E. Wolf, *Principles of Optics,* Pergamon Press, Oxford, 1975, Chapter 1.

[21] D. Boyers, A. Ho, Q. Li, M. Piestrup, M. Rice, R. Tatchyn, *Tests of variable-band multilayers designed for investigating optimal signal-to-noise versus artifact signal ratios in dual-energy digital subtraction angiography (DDSA) imaging systems,* Nucl. Instrum. Meth. A346, 565(1994).

[22] Art Toor, private communication.

[23] R. Tatchyn, P. Csonka, H. Kilic, H. Watanabe, A. Fuller, M. Beck, A. Toor, J. Underwood, and R. Catura, *Focusing of undulator light at SPEAR with a lacquer-coated mirror to power densities of* 10^9 *watts/cm*^{2}, SPIE Proceedings No. 733, 368-376(1986).

[24] Art Toor, private communication.

[25] J. Hajdu, *LCLS Scientific Advisory Committee Review*, SLAC, March 30, 2000.